



A hidden population of high-redshift double quasars unveiled by astrometry

Yue Shen 1,2 Xu-Ching Chen, Hsiang-Chih Hwang, Xin Liu 1,2, Nadia Zakamska, Masamune Oguri 64,5, Jennifer I-Hsiu Li 1, Joseph Lazio and Peter Breiding and Peter Breiding

Galaxy mergers occur frequently in the early Universe¹ and bring multiple supermassive black holes (SMBHs) into the nucleus, where they may eventually coalesce. Identifying post-merger-scale (that is, less than around a few kpc) dual SMBHs is a critical pathway to understanding their dynamical evolution and successive mergers2. Whereas serendipitous discovery of ~kpc-scale dual SMBHs at z < 1 is possible³, such systems are elusive at z > 2 but critical in constraining the progenitors of SMBH mergers. The redshift $z \approx 2$ also marks the epoch of peak activity of luminous quasars4, and therefore the probing of this spatial regime at high redshift is of particular importance in understanding the evolution of quasars. However, given stringent resolution requirements, there is currently no confirmed <10 kpc physical SMBH pair at z > 2 (refs. ⁵⁻⁸). Here, we report two sub-arcsec double quasars at z > 2 that were discovered from a targeted search with a novel astrometric technique, demonstrating a high success rate (>50%) in this systematic approach. These high-redshift double quasars could be the long-sought kpc-scale dual SMBHs, or sub-arcsec gravitationally lensed quasar images. One of these double quasars (at z=2.95) was spatially resolved with optical spectroscopy, and slightly favours the scenario of a physical quasar pair with a projected separation of 3.5 kpc (0.46"). Follow-up observations of double quasars discovered by this targeted approach will be able to provide observational constraints on kpc-scale dual SMBHs at z > 2.

The principles of the astrometry-based technique are threefold^{9,10}. First, the unresolved source contains multiple components. Second, these components have unsynchronized flux variations that cause astrometric jitter in the photocentre of the system. Third, this photocentre jitter is detectable with astrometric measurements. Extragalactic targets that fulfil these requirements include unresolved physical pairs (or multiples) of quasars and small-scale gravitationally lensed quasars. In the case of physical pairs, the variability of each quasar is stochastic and uncorrelated11; in the case of gravitationally lensed quasars, the variability from each image is also unsynchronized owing to lensing time delays¹². Assuming that the pair of quasars have comparable mean fluxes and root-mean-square (r.m.s.) fluctuations, the relation between the expected astrometric jitter σ_{astro} , the separation of the pair *D*, and the variability amplitude of the system is 10

$$\sigma_{
m astro} pprox rac{D}{2} rac{\sqrt{\langle \Delta f^2
angle}}{ar{f}} \,,$$
 (1)

where \bar{f} and $\sqrt{\langle \Delta f^2 \rangle}$ are the total mean and r.m.s. fluxes of the unresolved system. This relation can be generalized to non-equal-flux pairs, for which the expected astrometric jitter is reduced¹⁰, which renders this technique less efficient. Considering typical fractional r.m.s. fluctuations of quasars of ~10% (ref. 11), the expected astrometric jitter is ~10 mas for 0.2" separations, which corresponds to sub-kpc to kpc projected separations at cosmological distances.

Ground-based and seeing-limited imaging cannot easily resolve quasar pairs or lensed quasars with sub-arcsec separations, and diffraction-limited imaging with the Hubble Space Telescope (HST) or ground-based adaptive optics cannot probe large volumes. However, the anticipated astrometric jitter from such systems is well within the reach of the Gaia astrometry satellite^{13,14}, which covers the entire optical sky with roughly uniform photometric and astrometric sensitivities. This enables a novel targeted approach to systematically discover such systems with high efficiency.

We design a targeted search for sub-arcsec pairs among luminous quasars that appear to be singles in seeing-limited surveys, and focus on the z>2 regime in which mergers are expected to be more common. First, we select bright, spectroscopically confirmed quasars from the Sloan Digital Sky Survey (SDSS) 15,16 at z>2. We require that Gaia detects only a single source within a 3" radius of the SDSS position, and therefore the quasar is unresolved at the Gaia resolution of ~0.2"-0.8" depending on the scanning scheme of Gaia. The redshift cut ensures that host galaxy emission is negligible and that the optical light is dominated by the quasar light. At lower redshifts at which the more extended host galaxy is detectable with Gaia, the astrometric solution may be compromised given the scanning directions of Gaia and the astrometric modelling^{10,17}. Then, we restrict the selection to objects for which Gaia detects significant astrometric excess noise¹⁸—a proxy for the astrometric jitter signal expected from an unresolved quasar double. The full details of target selection are provided in the Methods. Our selection of small-scale quasar pairs using Gaia is therefore markedly different from the use of resolved multiple Gaia sources¹⁹, and can probe much smaller pair separations.

This astrometric selection with Gaia resulted in 15 candidates. Four of them were randomly observed by an HST Snapshot program (Methods and Extended Data Fig. 1). We show the two-band composite images of these four candidates (Fig. 1 and Extended Data Fig. 2). Two of them (J0749 and J0841) reveal two point-like cores separated by ~0.5" with comparable fluxes and similar colours, with no obvious detection of extended features. In addition,

¹Department of Astronomy, University of Illinois at Urbana-Champaign, Urbana, IL, USA. ²National Center for Supercomputing Applications, University of Illinois at Urbana-Champaign, Urbana, IL, USA. 3Department of Physics and Astronomy, Johns Hopkins University, Baltimore, MD, USA. 4Research Center for the Early Universe and Department of Physics, University of Tokyo, Tokyo, Japan. 5 Kavli Institute for the Physics and Mathematics of the Universe (Kavli IPMU), University of Tokyo, Tokyo, Japan. ⁹Jet Propulsion Laboratory, California Institute of Technology, Pasadena, CA, USA. ⁷Department of Physics and Astronomy, West Virginia University, Morgantown, WV, USA. $^{\boxtimes}$ e-mail: shenyue@illinois.edu

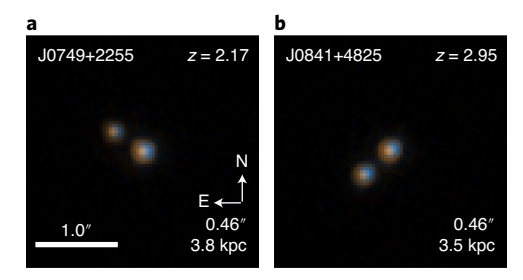


Fig. 1 | HST two-band composite images of two double quasars. a,b, The separations of resolved double cores in angular and physical units are marked. The double cores in J0749 (**a**) and J0841 (**b**) have similar colours, which indicates that both are most likely quasars, either from a physical pair or as multiple images of a gravitationally lensed quasar.

the optical spectra from SDSS (Fig. 2 and Extended Data Fig. 3) that enclose all light within a $2-3^{\prime\prime}$ diameter fibre rule out an obvious quasar–star superposition or (unrelated) projected quasar pairs. Therefore, these two objects are strongly favoured for physical quasar pairs or lensed quasars. Additional observations confirming their double-quasar origin are provided in Methods and Extended Data Fig. 4. The third object, J0905, has two resolved point-like components with different colours and a very small flux ratio in the blue band. Therefore, J0905 is most likely a quasar–star superposition that cannot be easily ruled out from the SDSS spectrum, as further reasoned in Methods. The remaining object, J1326, is a single point source under an HST resolution of ~0.1", which indicates that Gaia astrometric excess noise is caused by pairs within 0.1" or is due to unknown Gaia systematics. Extended Data Fig. 5 shows the imaging decomposition results of the HST data.

We estimate the frequency of z>2 SDSS quasars that are apparent singles in seeing-limited surveys but are in fact doubles (or multiples) on sub-arcsec scales by using the statistics from our targeted search with astrometry. Assuming that the frequency is not a function of limiting magnitude, we had 15 targets selected with Gaia astrometric excess noise for HST follow-up, out of ~11,000 parent quasars, or 0.14%. This is a hard lower limit, as most of these quasars could be doubles at smaller separations and/or their variability amplitude is low; therefore the astrometric jitter would be well below the Gaia astrometric excess noise cut that we imposed during target selection. Among the four randomly observed targets with HST, two are double quasars on sub-arcsec scales, which gives a success rate of 50%. This is again a lower limit, as the separation can be below the HST resolution of ~0.1" in the fourth object. The combined lower limit of the frequency is therefore ~0.1%. Incidentally, this rate is consistent with the estimated rate of <0.4% for lensed quasars at >1" image separations²⁰. We can also compare to the kpc-scale physical pair fraction extrapolated from small-scale quasar clustering measurements at z < 2 (ref. 21), which suggested a pair fraction of ~0.05% (Methods). The anticipated frequency of kpc-scale physical quasar pairs may be substantially higher at z > 2 (Methods).

To further illuminate the nature of the double quasars discovered by Gaia astrometry, we acquired optical slit spectroscopy for one of the double-cored targets (J084129.77 + 482548.5, referred to here as J0841) with Gemini under excellent seeing conditions. The system is spatially resolved in the slit spectroscopy (Methods and Extended Data Fig. 6) at the locations of the two HST cores. The two spatially resolved spectra (Fig. 2) are rather similar quasar spectra. The flux ratio of the two cores averaged over the optical spectral range is \sim 1.5, which is consistent with that measured from HST imaging.

Although there are spectral differences in the two cores of J0841 (Methods and Extended Data Fig. 7), notably in the strengths of the broad emission lines, the possibility of lensing cannot be ruled

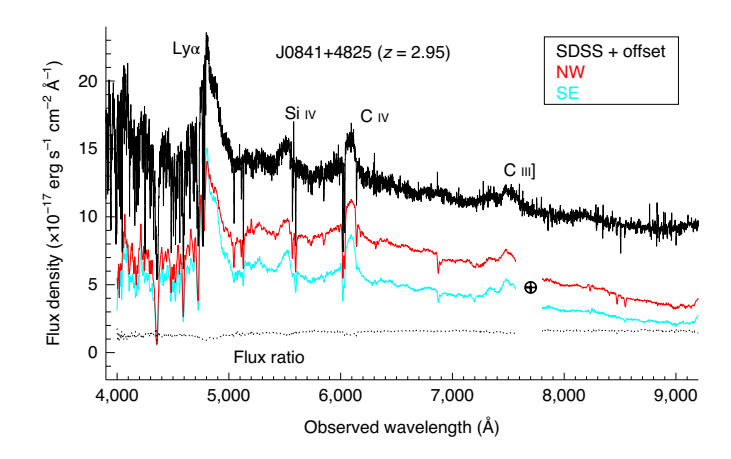
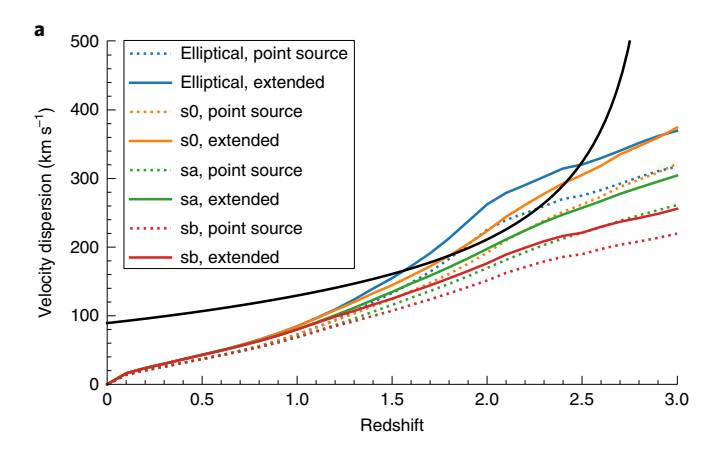


Fig. 2 | Spatially resolved optical spectroscopy of J0841. The red and cyan lines are for the northwestern (NW) and southeastern (SE) cores, respectively. The grey dotted line denotes the flux ratio between the two cores. The circled-cross symbol denotes the telluric absorption region masked out in the red and cyan spectra. The black line is the spectrum from SDSS (with offset for clarity) that covers both cores. The two cores have similar spectral appearances, albeit with differences in the strengths of the broad emission lines (Methods).

out conclusively. We therefore model the system as a gravitationally lensed quasar in which the lens galaxy is undetected in HST imaging (Methods). There are only three other gravitationally lensed double quasars with <0.8" separations known at z>2.5 (ref. ^{22–24}), all of which were serendipitously discovered, unlike J0841, which is from a targeted search. The black line in Fig. 3a is the required lens velocity dispersion at a given lens redshift. We further use the HST non-detection to place 3σ upper limits of the lens galaxy, indicated by the coloured lines, which lie below the lens model constraint at z<1.5. This suggests that a lens galaxy at z>1.5 is not ruled out by HST non-detections. We caution that our detection limit estimates for extended sources may be overly optimistic, and that more conservative non-detection limits will lead to less stringent constraints on the lensing hypothesis (see Methods for details).

In addition, we can estimate the lensing probability by using the abundance of lens galaxies and the impact parameters of the lensing system. The red line in Fig. 3b is the cumulative number of lenses that could have produced a lensed quasar as in J0841. Taking into account the parent quasar sample, the lensing magnification bias and the probability of observing the lensed quasar in our follow-up, we estimate a total probability of \sim 5% that J0841 is a doubly lensed quasar. Based on the same statistical arguments, we can estimate the total number of sub-arcsec lensed quasars expected from our parent sample to be \sim 2–3, which is fewer than the number of double quasars anticipated from our systematic search (Methods). However, given the uncertainties in the assumptions in our statistical arguments, the existing data are insufficient to rule out the possibility that the sub-arcsec double quasars discovered by astrometry are dominated by the lensed population.

Conversely, many observed high-redshift double quasars at >1" are physically associated rather than lensed images 6,8,25,26 , and our initial results with this systematic approach can place some interesting constraints on the <10 kpc dual supermassive black hole (SMBH) population at z>2. Our targeted search with Gaia astrometry preferentially selects pairs with projected ~kpc physical separations at z>2 and with comparable fluxes, that is, typically from major mergers. If we assume that all of the sub-arcsec pairs discovered with the astrometric technique are kpc-scale physical pairs on their way to coalescence, their frequency is ~0.1% among all optically selected z>2 quasars. As quasars light up stochastically,



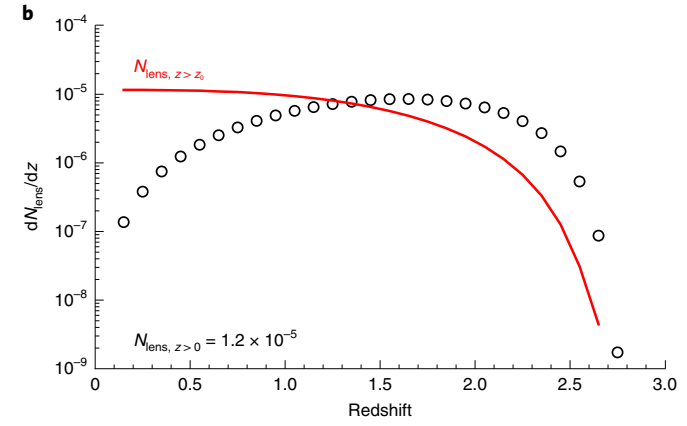


Fig. 3 | Lensing probability. a, The black line is the required stellar velocity dispersion for the lens at various redshifts. The different coloured lines are the 3σ upper limits from the non-detection of the lens galaxy in J0841 in HST F814W, for point sources (dotted lines) and extended sources (solid lines), respectively. **b**, The points are the differential number of lenses at various redshifts, estimated using the stellar velocity dispersion function and impact parameter for a hypothetical lensed quasar in J0841 (detailed in Methods). The red line is the cumulative number of lenses for lens redshift greater than the threshold.

not all kpc-scale dual SMBHs are both quasars at the same time, and we will observe only a fraction of them as quasar doubles. The duty cycle of quasars is roughly 1% at z>2 based on recent SDSS quasar clustering measurements²⁷, and we assume that being in a kpc-scale binary does not alter the duty cycle. Therefore, the frequency of ~kpc dual SMBHs among all optical quasars at z>2 would be ~10%. The dynamical evolution of the dual SMBH from tens of kpc to ~10 pc is determined by dynamical friction^{2,28}, although gas drag may not be negligible in high-redshift gas-rich mergers. With dynamical friction alone, in general the SMBH pair spends about a factor of ten less time²⁸ on hundreds of pc scales than on the kpc scales probed by our observations. Therefore, by extrapolating our results on kpc scales to scales a factor of ten smaller, we expect ~1% of z>2 optical quasars to be sub-kpc dual SMBHs, and ~0.01% of them will appear as sub-kpc double quasars.

An alternative scenario for J0841 is that it is a physical quasar pair, but not from the merger of two galaxies. High-redshift galaxies in formation are often clumpy²⁹, with massive clumps separated by up to 10 kpc. It is possible that these clumps, which constitute the bulk stellar mass of the galaxy, each contain an SMBH at the centre. The formation of these galactic clumps through disk instabilities may have also facilitated gas inflow within each clump to feed onto seed SMBHs. In this scenario, the growth of the two SMBHs may

be synchronous, resulting in rather similar spectral appearances and physical properties such as black hole mass when witnessed as a close pair of quasars. However, deep infrared imaging and kinematics studies are required to test this scenario of multiple SMBH formation in clumpy high-redshift galaxies.

The novel technique based on precision Gaia astrometry and physical causes of astrometric jitter in unresolved distant sources opens a new window to systematic discovery and characterization of sub-arcsec physical quasar pairs at high redshift, after the contamination from lensed quasars is properly quantified with detailed follow-up observations. This population of quasar pairs is expected to exist, but so far has been observationally elusive. The efficiency of this approach is demonstrated to be high based on follow-up observations with HST imaging and slit spectroscopy. The technique is most effective for pairs with comparable fluxes, which produce the most significant astrometric jitter in the systemic photocentre¹⁰. As spatially integrated spectroscopy can be used to rule out obvious quasar-star pairs, and as galaxies are generally too faint to affect the photocentre at z > 2, spatially resolved optical imaging provides strong evidence for the double quasar nature (either a physical pair or lensed images) to be confirmed by additional observations, as demonstrated here.

Further confirmation of quasar doubles selected with this technique but with separations below HST resolution can be achieved with the James Webb Space Telescope (with a factor of a few better resolution in the optical range than HST) and/or radio interferometry, as well as adaptive-optics-assisted near-infrared slit spectroscopy. In particular, near-infrared spectroscopy will cover narrow emission lines of these high-redshift quasars to identify potential velocity offsets in the narrow-line emission, which can also signal physical quasar pairs without the need to spatially resolve the pair³⁰. This targeted approach provides candidates with high purity, and enables efficient follow-up observations to confirm the nature of physical pairs or lensed images. In turn, the observations will lead to much improved statistics of high-redshift small-scale dual SMBHs, and to a much better understanding of the kpc to sub-kpc environment of high-redshift quasars and of the sub-arcsec lensed quasar population.

Methods

Varstrometry selection. Our technique combines astrometry and variability in unresolved quasar doubles, referred to as 'varstrometry' for convenience10,31. Gaia measures source properties with a window size¹³ of roughly 1.2" × 2.8". Depending on the scanning direction of Gaia, it is possible that close pairs with sub-arcsec separations are still unresolved and that Gaia measures the system as a single point source. However, ~80% of the pairs with separations ≳1" are resolved by Gaia Data Release 2 (DR2)32. Therefore, the varstrometry technique probes sub-arcsec separations in unresolved Gaia DR2 sources. The Gaia astrometric solution has an extra noise term, astrometric_excess_noise, that describes the r.m.s. residuals that cannot be accounted for by measurement uncertainties. With zero parallax and proper motion in the astrometric solution, this quantity is then equivalent to the r.m.s. astrometric jitter defined in equation (1) for unresolved quasar pairs or lensed images. At low redshift, extended host galaxy light and the random orientation of the galaxy relative to the Gaia scanning direction may induce additional systematic errors in the photocentre measurements that can contribute to astrometric_excess_noise as well

To select a clean sample to test the efficiency of the varstrometry technique in finding sub-arcsec double quasars, we start from the spectroscopically confirmed quasars from the SDSS DR7 and DR14 quasar catalogues 15,16 . We restrict the selection to $z\!>\!2$ quasars so that host galaxy emission is negligible in the Gaia G band and we require that there is only a single Gaia match within a 3'' radius of the SDSS position. We further limit the selection to the brightest quasars with $G\!<\!19.1$ so that Gaia can measure photometry and astrometry to superb precision, which yields 13,247 quasars. To ensure robust astrometric measurements, we further restrict to objects with Gaia visibility_periods_used $>\!8$, which yields 11,537 objects. We then select 15 of them with astrometric_excess_noise $>\!1.45$ mas. We visually inspect the SDSS spectra of the 15 targets and remove two objects with 0 bvious stellar features (therefore likely a quasar–star pair), and end up with 13 targets.

As a small number of quasars with high astrometric_excess_noise may fall slightly below the G=19.1 flux limit, we impose a secondary selection with

astrometric_excess_noise > 3 mas and G < 19.5. Only three additional targets meet these cuts, and one of them with stellar features in the SDSS spectrum is removed, which leaves two additional targets. These two targets have nearly identical Gaia magnitudes (G= 19.3) and astrometric_excess_noise. Our final target sample therefore includes 15 objects, and their distribution in the G magnitude versus astrometric_excess_noise plane is shown in Extended Data Fig. 1. For the parent sample statistics, however, we still use the sample of 11,537 objects with G < 19.1 that dominates our target selection, as the selection to G < 19.5 is highly incomplete. We note that one of the two confirmed double quasars, J0841, was from the ancillary selection. If we restrict our statistical constraints on the double-quasar frequency strictly to the main target selection, then we have a slightly lower success rate, >1/3 instead of >50%. The resulting double-quasar frequency in the parent quasar sample becomes slightly lower than ~0.1% but still roughly in line. As our statistical estimates are all approximate, we ignore this detail in our following analysis.

The Gaia magnitude and astrometric_excess_noise cuts in our selection are imposed both to reduce potential contamination from systematics and to yield a reasonable sample size for an HST program. If we were to lower these thresholds, we would have more candidates albeit with a potentially higher contamination rate. As we have confirmed a very high success rate with our stringent Gaia cuts, the next step would be to lower the Gaia magnitude cut and astrometric_excess_noise cut to increase the target sample size, and to quantify the success rate at these less stringent Gaia cuts.

With these Gaia astrometric parameters and the assumption of a total fractional photometric variability of 10%, equation (1) implies that our sample probes quasar doubles at separations between ~30 mas and ~1". At z=2, this angular separation range corresponds to projected separations between 250 pc and 8.5 kpc, which are more stringent limits than have been systematically explored before $^{5.68}$ at z>2. However, as SMBH pairs spend much more time on kpc scales than on smaller scales owing to dynamical friction, we expect that our methodology will preferentially discover kpc-scale double quasars.

One caveat in the above derivation is that the mapping from astrometric jitter to physical separations is approximate at best. Because Gaia has not released time-resolved photocentre measurements and photometry, our analysis relied on published surrogates for the photometric variability and astrometric jitter. In addition, the assumption that the fractional variability is similar for both components may break down. Therefore, we do not necessarily expect good agreement between the HST-measured pair separation and the predicted separation via equation (1). It is also possible that a sub-arcsec pair, while fully within the astrometry measurement window, would suffer more from Gaia astrometric systematics than single sources would. Nevertheless, the targeting of high-z quasars with significant Gaia astrometric excess noise efficiently reveals systems with sub-arcsec companions that have compromised the Gaia astrometric solution, which justifies this overall targeting strategy.

Follow-up observations. The 15 SDSS–Gaia quasars were then included in an HST Snapshot program to acquire two-band optical imaging in UVIS/F475W and UVIS/F814W, with typical exposure times of 360 s (400 s) in F475W (F814W). Submitted targets are observed in HST Snapshot programs only if those programs fill the 'gaps' between regularly scheduled programs. Four of the 15 targets were randomly observed, with three showing doubles (Fig. 1 and Extended Data Fig. 2). The success rate is therefore very high, which demonstrates the efficiency of the varstrometry technique. The optical spectrum for J0841 is shown in Fig. 2, and the SDSS spectra for the remaining three targets are shown in Extended Data Fig. 3. Additional properties of the four targets are provided in Supplementary Table 1.

Image decomposition of the HST data with GALFIT³³ indicates that all components in resolved doubles are consistent with point sources, with no evidence of extended host or additional components between resolved double cores. For the three resolved double cores, we measure a flux ratio in F475W (F814W) of 4.4 (3.6) for J0749, 1.3 (1.7) for J0841 and 46 (4.5) for J0905, with 1σ fractional uncertainties of <10%. The GALFIT results are shown in Extended Data Fig. 5.

We obtained Gemini director's discretionary time (DDT) for one of the three HST-resolved doubles, J0841. This particular target was chosen owing to visibility constraints and to the limited amount of DDT available for the highest image quality (the top 20%), which is necessary to spatially resolve the double from ground-based seeing-limited observations. With the approved DDT, J0841 was observed on 2020 May 21 UT by using optical slit spectroscopy with the Gemini multi-object spectrograph (GMOS) at Gemini-North (program GN-2020A-DD-106). We chose optical spectroscopy over near-infrared spectroscopy to ensure the detection of both cores in this high-redshift quasar, but future near-infrared slit spectroscopy to spatially resolve the narrow emission lines is warranted. The observations were carried out under superb conditions, with a seeing full width at half maximum (FWHM) of ~0.4"-0.5", which was sufficient to resolve the double. We adopted the long slit with the R150 grating and a 0.75" slit width. It offers a spectral resolution of $R \approx 420$ (corresponding to $\sigma_{\rm inst} \approx 210 \ \rm km \ s^{-1}$), which spans the observed ~400–950 nm with a pixel scale of 1.93 Å pixel⁻¹ along the wavelength direction. The slit was placed across the two cores along a position angle of 132.0°. The total exposure time was 1,848 s, which

was divided into two individual exposures dithered at two central wavelengths (700 nm and 720 nm) to cover the CCD chip gaps and to help reject cosmic rays. We reduced the data following standard IRAF procedures⁵⁴ by using the PyRAF package (http://go.nature.com/3bzVBjg). The two-dimensional (2D) spectra were wavelength-calibrated using CuAr lamp lines and stored in vacuum wavelength. The white dwarf EG 131 was observed as the standard star for flux calibration during the same night.

To spatially resolve the double cores, we first collapse the 2D spectrum along the wavelength direction to construct a spatial profile (Extended Data Fig. 6). For J0841 at z = 2.95, the optical emission is dominated by the accretion disk and broad emission lines, and therefore both cores can be treated as point sources with the same point spread function (PSF) determined by seeing. The two cores are resolved clearly in the 2D spectrum, and the wavelength-collapsed profile provides a robust measure of the seeing profile. We found that a single Gaussian fits the PSF core well, with a measured FWHM of 0.4", which is consistent with the seeing at the time of the observations, and with a spatial offset of 5.8 pixels (or ~0.47") between the two cores, which is consistent with the separation measured from HST imaging. With the measured PSF, we then decompose the two cores at each wavelength to extract the one-dimensional (1D) spectra for both cores. We use a single Gaussian for each component, with the separation and Gaussian dispersion fixed from the spatial profile derived earlier, but allowing the amplitude of each Gaussian to vary in case the two components have different spectral shapes. The spatially decomposed 1D spectra for the two cores are shown in Fig. 2.

The two spectra are very similar in appearance with nearly identical redshifts, except for subtle differences in spectral shape, strengths of certain intervening absorption lines, and strengths of broad emission lines (Extended Data Fig. 7). In general, these spectral differences can be explained in the lensing scenario, but the different flux ratios in the continuum and in the broad emission lines require a microlensing event³⁵, thereby reducing the lensing probability. A simpler explanation for the spectral dissimilarity is that J0841 is a physical quasar pair. With the assumption that the two quasars have the same black hole mass, the factor of 1.5 difference in continuum luminosity will not be reflected in their broad-line width difference, because broad-line width scales as $L^{1/4}$ if the broad-line region is virialized36. Bearing in mind the large (~0.4 dex) systematic uncertainties, we estimate black hole masses for the two quasars in J0841 by using the single-epoch virial mass method³⁶ as $10^{9.4\pm0.4}M_{\odot}$ (southeastern) and $10^{9.6\pm0.4}M_{\odot}$ (northwestern), for which the spectral fits were performed by using the public QSOFIT code3 and the mass errors represent 1σ standard deviations and are dominated by systematic uncertainties.

For J0749, although we have not obtained spatially resolved spectra, a 15 GHz (2 cm wavelength) image obtained with the Very Long Baseline Array (VLBA) shows both cores (Extended Data Fig. 4), which confirms its double-quasar nature. These two quasars must be at the same redshift given the lack of multiple emission-line systems in the SDSS spectrum. The full analysis of these VLBA data (including data in additional frequency bands) will be presented elsewhere.

Lensing model of J0841. We perform simple lens modelling by using a singular isothermal sphere (SIS), which is shown to be a good approximation for sub-arcsec lensing. The SIS model constrains the velocity dispersion of the lens galaxy as a function of the unknown lens redshift, as shown by the black line in Fig. 3a. From the HST non-detection of the lens (with exposure time of 400 s in F814W), we constrain the 3σ upper limit of the galaxy luminosity for a range of morphological types with different spectral shapes. For each galaxy type, we consider both a point source and an extended source. For the point source case, the 3σ optimal extraction corresponds to a limiting AB magnitude of 27 in F814W. For the extended source case, we assume that all light is uniformly distributed within a 0.2'' radius (that is, filling the area between the two cores) and reaches a limiting AB surface brightness of 24.1 mag arcsec⁻². We then convert the galaxy luminosity to velocity dispersion by using empirical relations measured for local galaxies. The scatter in velocity dispersion at fixed luminosity is $\lesssim 25\%$ and we assume no evolution in these scaling relations.

We note that the limits for the extended source case are optimistic, as the lens galaxy can be more extended and blend into the PSF wings of the quasars. For this reason, we proceed with caution on our lensing probability assessment. This exercise is presented as a general methodology to test the lensing hypothesis, even though the current data are insufficient to draw definitive conclusions.

The upper limits on the velocity dispersion inferred from the HST non-detection are plotted against redshift in Fig. 3a for different galaxy types. Although the HST imaging is not deep enough, these upper limits meaningfully rule out a lens at z < 1.5. Lenses at higher redshifts are still possible considering the uncertainties in the estimated upper limits from HST non-detection. To further evaluate this possibility, we estimate the number of galaxies with sufficient velocity dispersion along the line of sight towards J0841 from random superposition. We use the stellar velocity dispersion function measured for local early-type galaxies⁴¹, which shows only mild evolution towards $z \approx 2$. In the case of an SIS lens, the flux ratio of two images is given by r = (1+y)/(1-y), where y is the angular separation between the source and the lens centre normalized by the Einstein radius. For the flux ratio of r = 1.5, we have y = 0.2, so the impact parameter required to reproduce the observed flux ratio is 0.046''. Our selection strategy is able to randomly

discover lensed images with separations within a factor of two of the observed $\sim\!0.4''$ separation. The lower limit is set by the HST resolution and the upper limit is set by Gaia, that is, larger separations will be resolved by Gaia. This image separation range corresponds to a range of SIS velocity dispersions that enclose a factor of $\sqrt{2}$ around the fiducial value, over which we integrate to obtain the lens galaxy number density at given lens redshift. The cumulative number of random intercepting galaxies at redshifts greater than a threshold is shown as the red line in Fig. 3b. The expected number is therefore $\sim\!6\!\times\!10^{-6}$ for $a\,z\!\gtrsim\!1.5$ lens. If we adopt a more conservative sensitivity (for example, by reducing by one magnitude) for the lens galaxy in the extended-source case, the lensing modelling can rule out a lens galaxy at $z\!>\!1.2$ (as opposed to $z\!>\!1.5$). The corresponding cumulative lens probability would increase from $6\!\times\!10^{-6}$ to $8\!\times\!10^{-6}$.

We further estimate the expected total number of sub-arcsec doubly lensed quasars with comparable image flux ratios, for the parent population of z > 2quasars. As the lensing probability increases towards higher source redshift, we can conservatively use the single-lensing probability estimated earlier for J0841 at $z \approx 3$. There are ~11,000 parent z > 2 quasars. To estimate the boost factor in source number density owing to lensing magnification bias⁴³, we use the latest optical quasar luminosity function measured⁴⁴ at z>2 to derive a boost factor of ~30. Therefore, we expect ~2-3 doubly lensed quasars out of the ~11,000 parent quasars. Our program revealed that at least half of the 15 quasars with the highest varstrometry signals should be sub-arcsec double quasars, which already exceeds the lensing expectation with this subsample of 15 objects alone. Considering that our selection is by no means complete, the general population of sub-arcsec double quasars at z > 2 may be too abundant to be explained by the lensed population. However, as mentioned earlier, the uncertainties in the non-detection limits make it difficult to rule out the possibility that these double quasars are dominated by the lensing population. Deeper limits (preferentially from infrared imaging) are required to improve this statistical constraint.

We now roughly estimate the probability that J0841 is an expected lensed quasar from our lensing probability analysis. Although the efficiency of our varstrometry selection of high-redshift quasar doubles is high (≥50%), we cannot formally estimate the completeness of the selection technique owing to the lack of detailed knowledge on Gaia time series data, astrometric modelling, the unknown distributions of pair separations, and variability amplitudes. Nevertheless, we do not expect that the completeness is very high, as the technique is likely to miss most genuine sub-arcsec pairs with smaller astrometric jitter. We do not expect the completeness to be very low either (<10%), otherwise there may be an overabundance of sub-kpc dual SMBHs. Therefore, we assume a reasonable completeness of 50% for our selection, which means that the 15 HST targets should include one sub-arcsec lensed quasar. The probability that it happens to be observed in the four randomly observed targets is 27% (that is, $1 - C_{14}^4/C_{15}^4$). Therefore, the total probability of J0841 being a lensed quasar is 0.27. The conditioned probability that J0841 is a lensed quasar but also at z > 2.8 is further reduced to $0.27(2,242/11,537) \approx 0.05$, where 2,242 is the number of z > 2.8 quasars in the parent sample. There is therefore still a small probability of J0841 being a lensed quasar. As we have likely underestimated the total number of lensed quasars in our sample, the actual probability of J0841 being a lensed quasar could be significantly higher, but deep infrared imaging is required to confirm the required lens in J0841.

Implications from small-scale quasar clustering. The expected physical pair frequency can be estimated from small-scale quasar clustering measurements^{8,21}. Although there is no such clustering measurement on kpc scales, we use existing measurements at z < 2 and larger scales to derive some crude estimates. The small-scale quasar pair sample in ref. 21 enabled the measurement of the quasar correlation function on ≥15 kpc projected scales. Below ~50 kpc, there is evidence that the three-dimensional correlation function steepens to an r^{-3} power law, which would imply a constant pair fraction for each decade in scale. Based on the pair statistics from that work and with the assumption that their pair sample is complete, the extrapolated pair fraction on kpc scale is then ~0.05%. A somewhat higher pair fraction of $\sim 0.26\% \pm 0.18\%$ was recently reported based on ground-based imaging and spectroscopic follow-up⁴⁵. Furthermore, it is possible that the abundance of kpc-scale quasar pairs is much greater at z>2 given the increased specific merger rate and the enhanced probability that both SMBHs are quasars owing to merger-induced fuelling. This possibility is particularly relevant for the luminous quasars at z > 2, as in our bright Gaia sample. Therefore, we may expect a much higher kpc-scale quasar pair fraction at z>2, which will be tested with our systematic search using varstrometry.

J0905 as a quasar-star superposition. The colour discrepancy in the double cores in J0905 suggests that the fainter and redder component is a star. The measured F475W-F814W colour for the redder component is consistent with an M2V star. We add an M2V star spectrum to the SDSS quasar spectrum of J0905 by fixing the flux ratio in the F814W band. The predicted flux ratio in the F475W band is 0.02, which is consistent with that measured from HST data, and the predicted flux ratio in the Gaia G band is 0.1. The stellar absorption features of the star are difficult to identify given the flux errors. Therefore, we could not have rejected J0905 as a quasar-star superposition from the SDSS spectrum.

Data availability

The SDSS spectrum for J0841 is publicly available at https://www.sdss.org/. The HST data are publicly available via the Mikulski Archive for Space Telescopes (MAST) at https://archive.stsci.edu with program no. HST-GO-15900. The raw data for the Gemini spectrum are publicly available at https://archive.gemini.edu/ with program ID GN-2020A-DD-106, and the reduced spectrum is provided in the data for Fig. 2. The catalogue data for parent SDSS quasars are available in refs. ^{15,16}, and the astrometric data are publicly available from Gaia DR2 at https://gea.esac.esa.int/archive/. Additional data (preliminary VLBA images) that support the plots within this paper and other findings of this study are available from the corresponding author upon reasonable request. Source data are provided with this paper.

Code availability

The GALFIT code used to decompose the HST images is publicly available at https://users.obs.carnegiescience.edu/peng/work/galfit/galfit.html.

Received: 19 October 2020; Accepted: 9 February 2021; Published online: 01 April 2021

References

- 1. Duncan, K. et al. Observational constraints on the merger history of galaxies since $z\approx 6$: probabilistic galaxy pair counts in the CANDELS fields. *Astrophys. J.* **876**, 110 (2019).
- Begelman, M. C., Blandford, R. D. & Rees, M. J. Massive black hole binaries in active galactic nuclei. *Nature* 287, 307–309 (1980).
- Komossa, S. et al. Discovery of a binary active galactic nucleus in the ultraluminous infrared galaxy NGC 6240 using Chandra. Astrophys. J. Lett. 582, L15–L19 (2003).
- Richards, G. T. et al. The Sloan Digital Sky Survey quasar survey: quasar luminosity function from Data Release 3. Astron. J. 131, 2766–2787 (2006).
- Hennawi, J. F. et al. Binary quasars in the Sloan Digital Sky Survey: evidence for excess clustering on small scales. Astron. J. 131, 1–23 (2006).
- Hennawi, J. F. et al. Binary quasars at high redshift. I. 24 new quasar pairs at z~3-4. Astrophys. J. 719, 1672–1692 (2010).
- More, A. et al. The SDSS-III BOSS quasar lens survey: discovery of 13 gravitationally lensed quasars. Mon. Not. R. Astron. Soc. 456, 1595–1606 (2016).
- Eftekharzadeh, S. et al. Clustering on very small scales from a large sample of confirmed quasar pairs: does quasar clustering track from Mpc to kpc scales? Mon. Not. R. Astron. Soc. 468, 77–90 (2017).
- Liu, Y. Finding binary active galactic nuclei candidates by the centroid shift in imaging surveys. II. Testing the method with SDSS J233635.75-010733.7. Astron. Astrophys. 592, L4 (2016).
- Hwang, H.-C. et al. Varstrometry for off-nucleus and dual sub-kpc AGN (VODKA): methodology and initial results with Gaia DR2. Astrophys. J. 888, 73 (2020).
- MacLeod, C. L. et al. Modeling the time variability of SDSS Stripe 82 quasars as a damped random walk. Astrophys. J. 721, 1014–1033 (2010).
- Refsdal, S. On the possibility of determining Hubble's parameter and the masses of galaxies from the gravitational lens effect. *Mon. Not. R. Astron. Soc.* 128, 307 (1964).
- 13. Gaia Collaboration. The Gaia mission. Astron. Astrophys. 595, A1 (2016).
- Gaia Collaboration. Gaia Data Release 2. Summary of the contents and survey properties. Astron. Astrophys. 616, A1 (2018).
- Shen, Y. et al. A catalog of quasar properties from Sloan Digital Sky Survey Data Release 7. Astrophys. J. Suppl. Ser. 194, 45 (2011).
- Pâris, I. et al. The Sloan Digital Sky Survey quasar catalog: fourteenth data release. Astron. Astrophys. 613, A51 (2018).
- Lindegren, L. et al. Gaia Data Release 2. The astrometric solution. Astron. Astrophys. 616, A2 (2018).
- Lindegren, L. et al. The astrometric core solution for the Gaia mission. Overview of models, algorithms, and software implementation. *Astron. Astrophys.* 538, A78 (2012).
- Lemon, C. A., Auger, M. W., McMahon, R. G. & Koposov, S. E. Gravitationally lensed quasars in Gaia: I. Resolving small-separation lenses. Mon. Not. R. Astron. Soc. 472, 5023–5032 (2017).
- Pindor, B., Turner, E. L., Lupton, R. H. & Brinkmann, J. Determining the lensing fraction of SDSS quasars: methods and results from the Early Data Release. Astron. J. 125, 2325–2340 (2003).
- Kayo, I. & Oguri, M. Very small scale clustering of quasars from a complete quasar lens survey. Mon. Not. R. Astron. Soc. 424, 1363–1371 (2012).
- Bahcall, J. N., Maoz, D., Schneider, D. P., Yanny, B. & Doxsey, R. Hubble Space Telescope imaging of the large-redshift gravitational lens candidate 1208+1011. Astrophys. J. Lett. 392, L1 (1992).
- 23. Irwin, M. J., Ibata, R. A., Lewis, G. F. & Totten, E. J. APM 08279 + 5255: an ultraluminous broad absorption line quasar at a redshift z = 3.87. Astrophys. J. 505, 529-535 (1998).
- 24. Fan, X. et al. The discovery of a gravitationally lensed quasar at z=6.51. *Astrophys. J. Lett.* 870, L11 (2019).

- 25. Djorgovski, S. Quasar pairs at large redshifts. ASP Conf. Ser. 21, 349-353 (1991).
- Kochanek, C. S., Falco, E. E. & Muñoz, J. A. Why quasar pairs are binary quasars and not gravitational lenses. *Astrophys. J.* 510, 590–596 (1999).
- Eftekharzadeh, S. et al. Clustering of intermediate redshift quasars using the final SDSS III-BOSS sample. Mon. Not. R. Astron. Soc. 453, 2779–2798 (2015).
- 28. Yu, Q. Evolution of massive binary black holes. Mon. Not. R. Astron. Soc. 331, 935-958 (2002).
- Elmegreen, B. G. et al. Bulge and clump evolution in Hubble Ultra Deep Field clump clusters, chains and spiral galaxies. Astrophys. J. 692, 12–31 (2009).
- 30. Liu, X., Greene, J. E., Shen, Y. & Strauss, M. A. Discovery of four kpc-scale binary active galactic nuclei. *Astrophys. J. Lett.* 715, L30–L34 (2010).
- Shen, Y., Hwang, H.-C., Zakamska, N. & Liu, X. Varstrometry for off-nucleus and dual sub-kpc AGN (VODKA): how well centered are low-z AGN? Astrophys. J. Lett. 885, L4 (2019).
- Arenou, F. et al. Gaia Data Release 2. Catalogue validation. Astron. Astrophys. 616, A17 (2018).
- Peng, C. Y., Ho, L. C., Impey, C. D. & Rix, H.-W. Detailed decomposition of galaxy images. II. Beyond axisymmetric models. *Astron. J.* 139, 2097–2129 (2010).
- Tody, D. The IRAF data reduction and analysis system. Proc. SPIE 627, 733 (1986).
- Sluse, D. et al. Microlensing of the broad line region in 17 lensed quasars. Astron. Astrophys. 544, A62 (2012).
- 36. Shen, Y. The mass of quasars. Bull. Astron. Soc. India 41, 61-115 (2013).
- 37. Shen, Y. et al. The Sloan Digital Sky Survey Reverberation Mapping project: sample characterization. *Astrophys. J. Suppl. Ser.* **241**, 34 (2019).
- Oguri, M. The image separation distribution of strong lenses: halo versus subhalo populations. Mon. Not. R. Astron. Soc. 367, 1241–1250 (2006).
- Kinney, A. L. et al. Template ultraviolet to near-infrared spectra of star-forming galaxies and their application to K-corrections. Astrophys. J. 467, 38 (1996).
- 40. Bernardi, M. et al. Early-type galaxies in the Sloan Digital Sky Survey. II. Correlations between observables. *Astron. J.* **125**, 1849–1865 (2003).
- Sheth, R. K. et al. The velocity dispersion function of early-type galaxies. Astrophys. J. 594, 225–231 (2003).
- Bezanson, R. et al. Redshift evolution of the galaxy velocity dispersion function. Astrophys. J. Lett. 737, L31 (2011).
- Oguri, M. Strong gravitational lensing of explosive transients. Rep. Prog. Phys. 82, 126901 (2019).
- Ross, N. P. et al. The SDSS-III Baryon Oscillation Spectroscopic Survey: the quasar luminosity function from Data Release Nine. Astrophys. J. 773, 14 (2013).
- Silverman, J. D. et al. Dual supermassive black holes at close separation revealed by the Hyper Suprime-Cam Subaru Strategic Program. *Astrophys. J.* 899, 154 (2020).

Acknowledgements

Support for the work by Y.S. was provided by an Alfred P. Sloan Research Fellowship and by National Science Foundation (NSF) grant no. AST-2009947. The work by M.O. was

supported by the World Premier International Research Center Initiative (WPI Initiative) of the Japanese Ministry of Education, Culture, Sports, Science and Technology (MEXT) and by the Japan Society for the Promotion of Science (KAKENHI grant nos. JP18K03693, JP20H00181 and JP20H05856). This work is partially supported by a Scialog program sponsored jointly by Research Corporation for Science Advancement and the Heising-Simons Foundation. The NANOGrav project receives support from the NSF Physics Frontiers Center (award no. 1430284). Part of this research was carried out at the Jet Propulsion Laboratory, California Institute of Technology, under a contract with the National Aeronautics and Space Administration. We thank J. Blakeslee for granting us Gemini DDT. Observations were obtained at the international Gemini Observatory, a program of NSF's NOIRLab, which is managed by the Association of Universities for Research in Astronomy (AURA) under a cooperative agreement with the NSF on behalf of the Gemini Observatory partnership: the NSF (United States), National Research Council (Canada), Agencia Nacional de Investigación y Desarrollo (Chile), Ministerio de Ciencia, Tecnología e Innovación (Argentina), Ministério da Ciência, Tecnologia, Inovações e Comunicações (Brazil) and Korea Astronomy and Space Science Institute (Republic of Korea). Observations made with the NASA/ESA Hubble Space Telescope were obtained at the Space Telescope Science Institute, which is operated by AURA under NASA contract no. NAS 5-26555. These observations are associated with program no. GO-15900. The National Radio Astronomy Observatory is a facility of the NSF that is operated under a cooperative agreement by the Associated Universities corporation.

Author contributions

Y.S. designed the project and led the analysis and manuscript writing; X.L. led the Gemini program and Y.-C.C. reduced the Gemini spectra; H.-C.H. and N.Z. led the HST program; M.O. led the lensing analysis; J.I.-H.L. performed the HST imaging analysis; X.L., Y.-C.C., J.L. and P.B. contributed to the VLBA data; all authors contributed to the science interpretation.

Competing interests

The authors declare no competing interests.

Additional information

Extended data is available for this paper at https://doi.org/10.1038/s41550-021-01323-1.

Supplementary information The online version contains supplementary material available at https://doi.org/10.1038/s41550-021-01323-1.

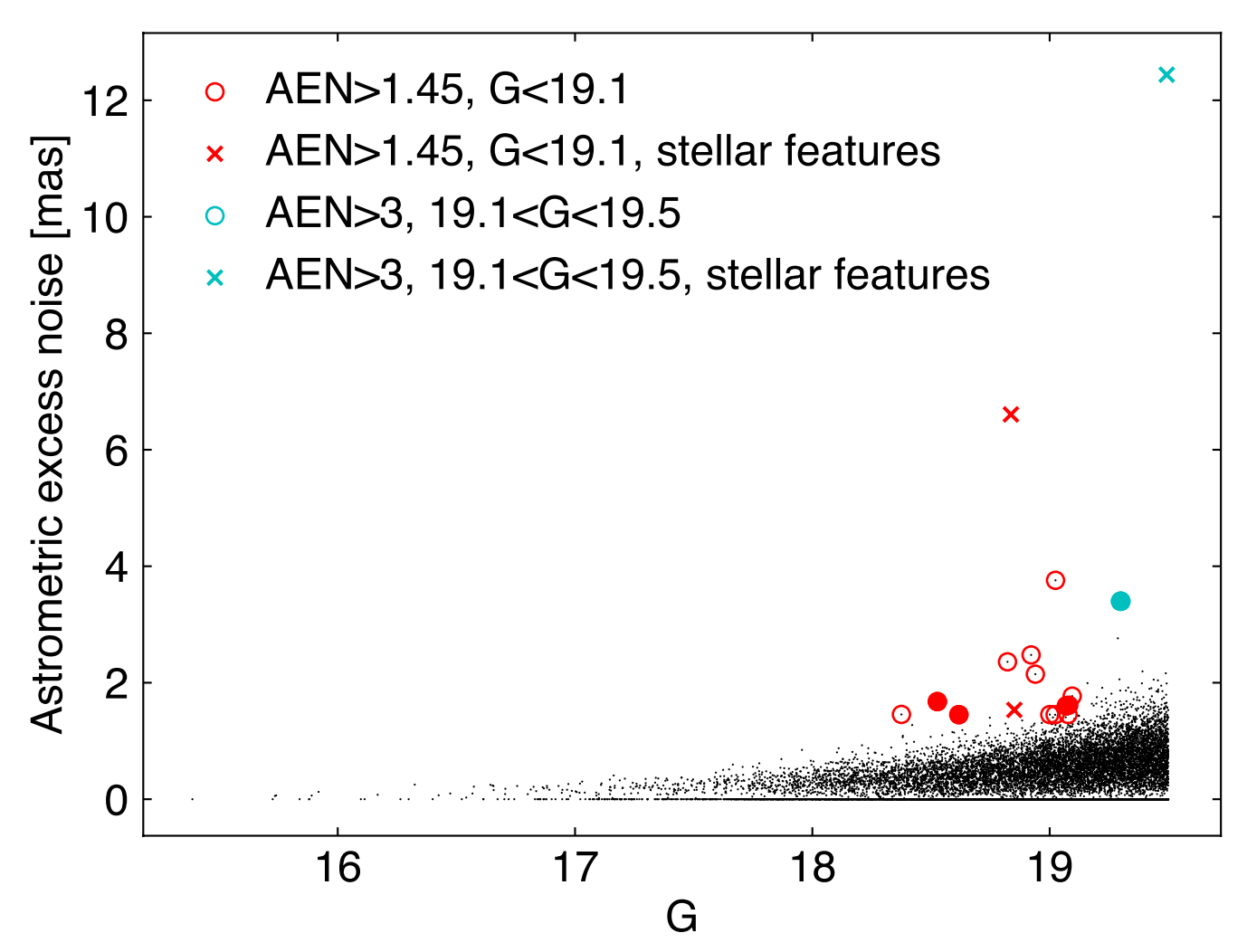
Correspondence and requests for materials should be addressed to Y.S.

Peer review information *Nature Astronomy* thanks the anonymous reviewers for their contribution to the peer review of this work.

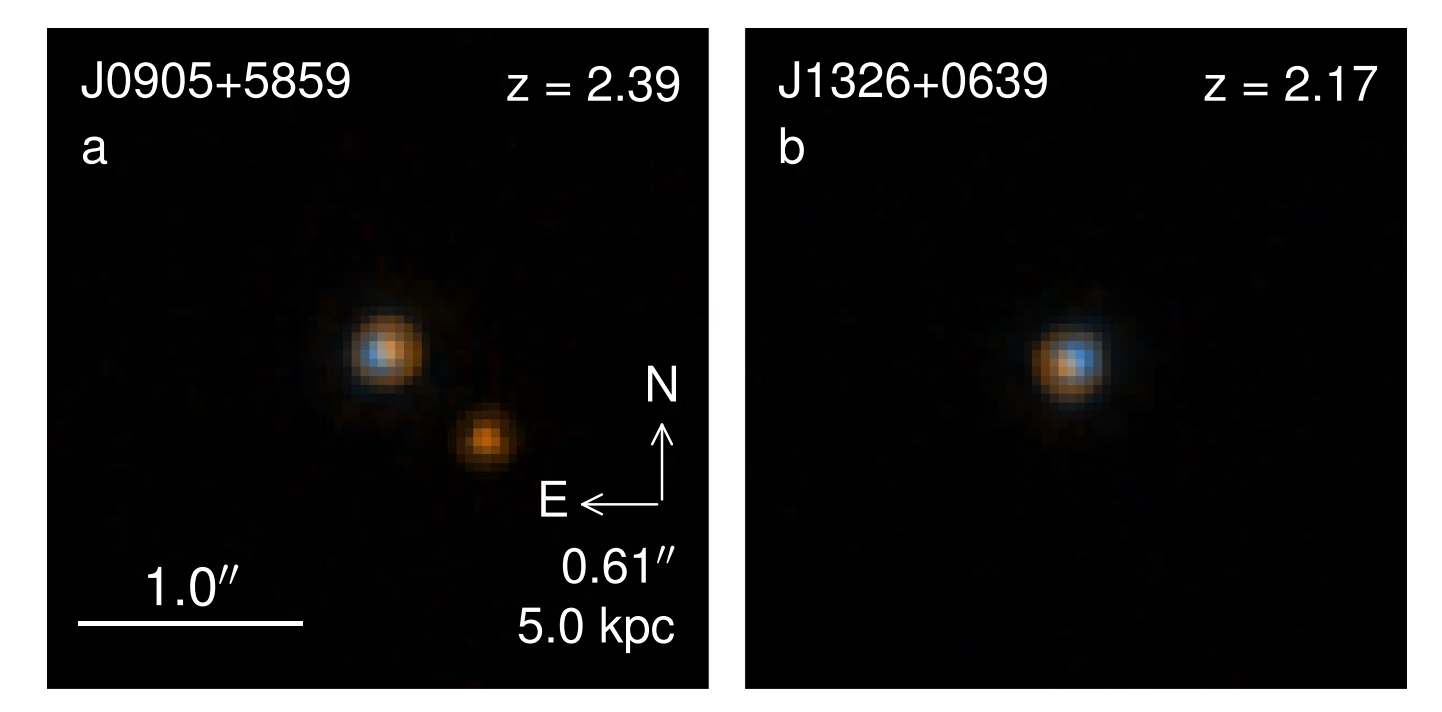
Reprints and permissions information is available at www.nature.com/reprints.

Publisher's note Springer Nature remains neutral with regard to jurisdictional claims in published maps and institutional affiliations.

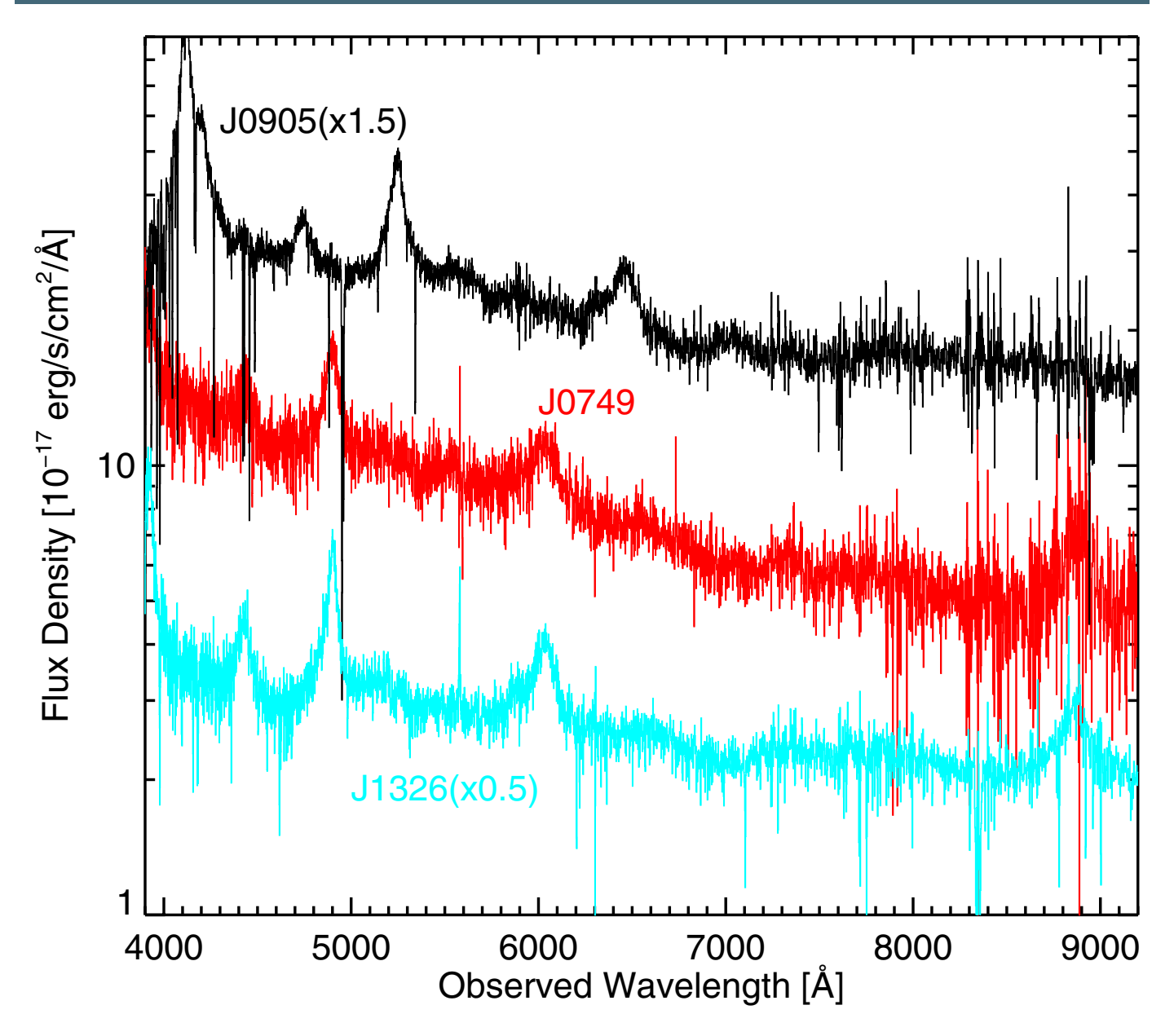
© The Author(s), under exclusive licence to Springer Nature Limited 2021



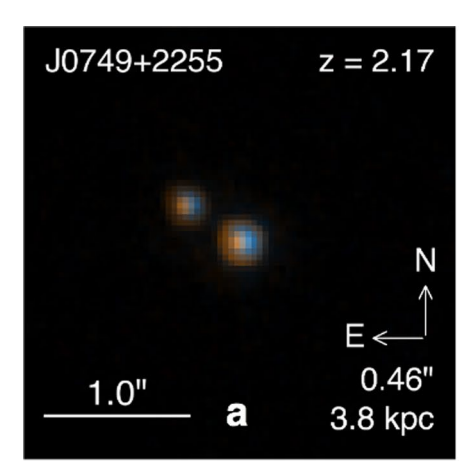
Extended Data Fig. 1 | Gaia selection of candidate double quasars. The black dots are the parent z > 2 SDSS quasars with single Gaia matches. The red and cyan circles are our final sample of 15 targets (there are two objects in cyan circles that overlap with each other), and the crosses are excluded objects based on apparent spectral features that indicate a star-quasar superposition (see details of target selection in Methods). Measurement uncertainties are negligible. Most of the objects at G > 19.1 with high astrometric excess noise are excluded from our extended target selection (only the cyan circles are selected). The four targets that have been followed up by HST are indicated by filled circles, and the remaining targets are indicated by open circles.

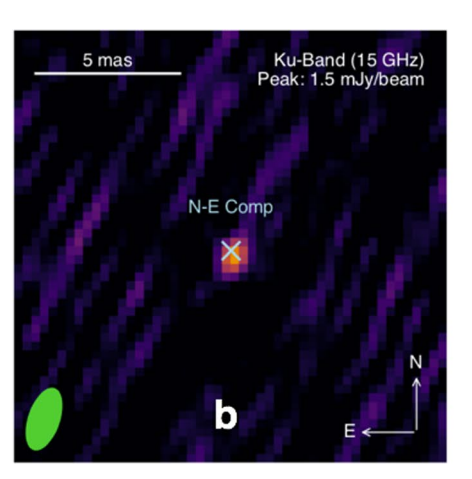


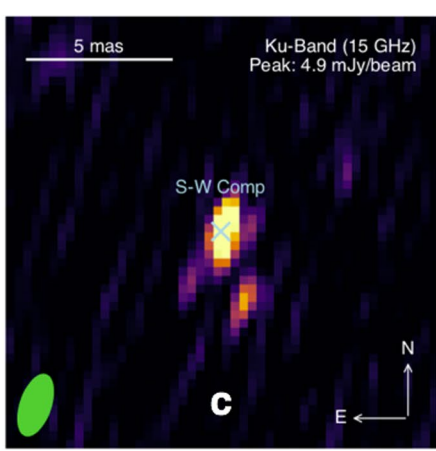
Extended Data Fig. 2 | HST 2-band composite images of the remaining two targets. The different colors in the two cores in J0905 suggest it is a quasar-star superposition, and J1326 is not resolved at the HST resolution of ~0.1°.



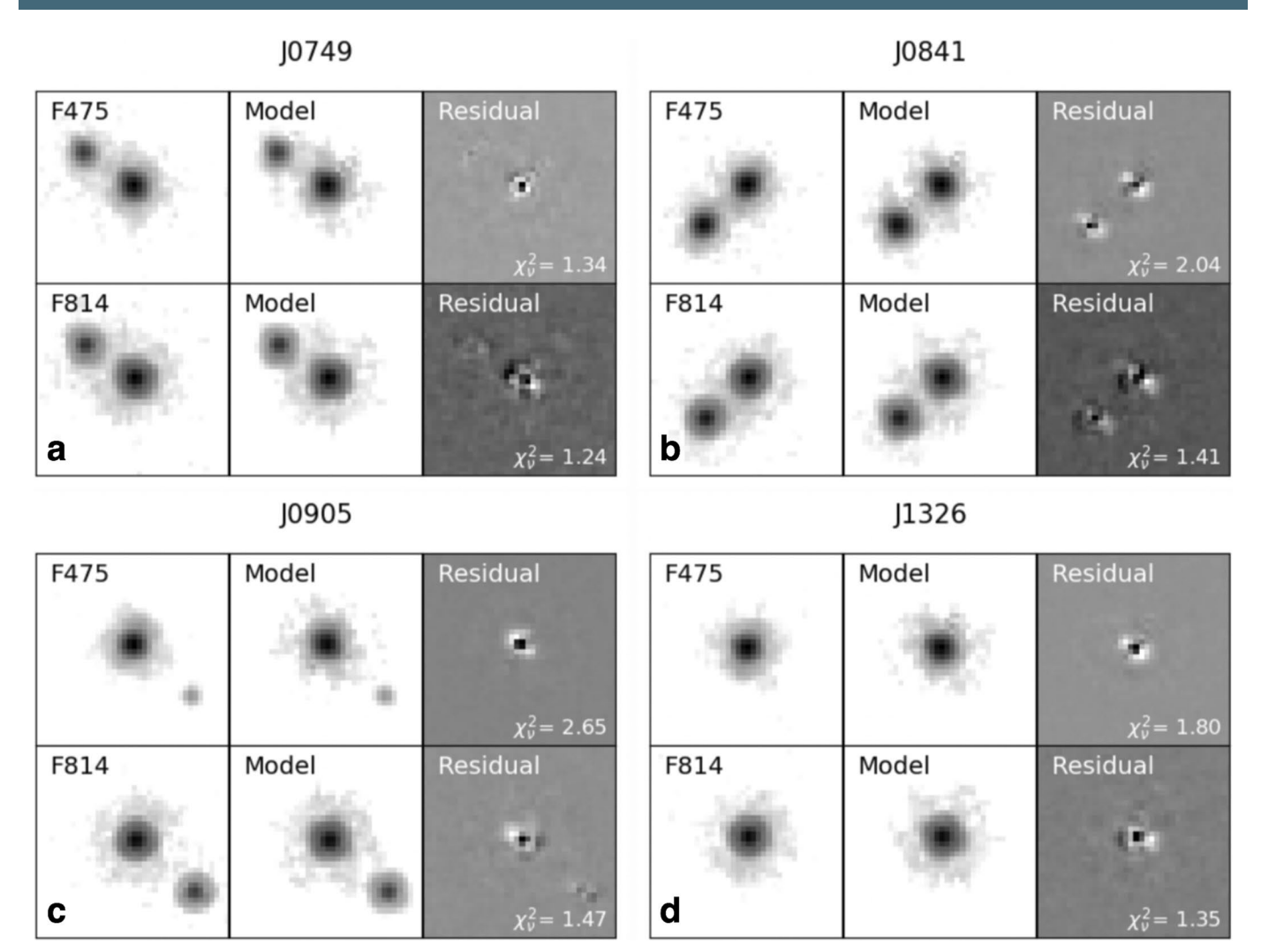
Extended Data Fig. 3 | SDSS spectra for three targets observed by HST. The flux densities of J0905 and J1326 have been scaled for the clarity of the figure.



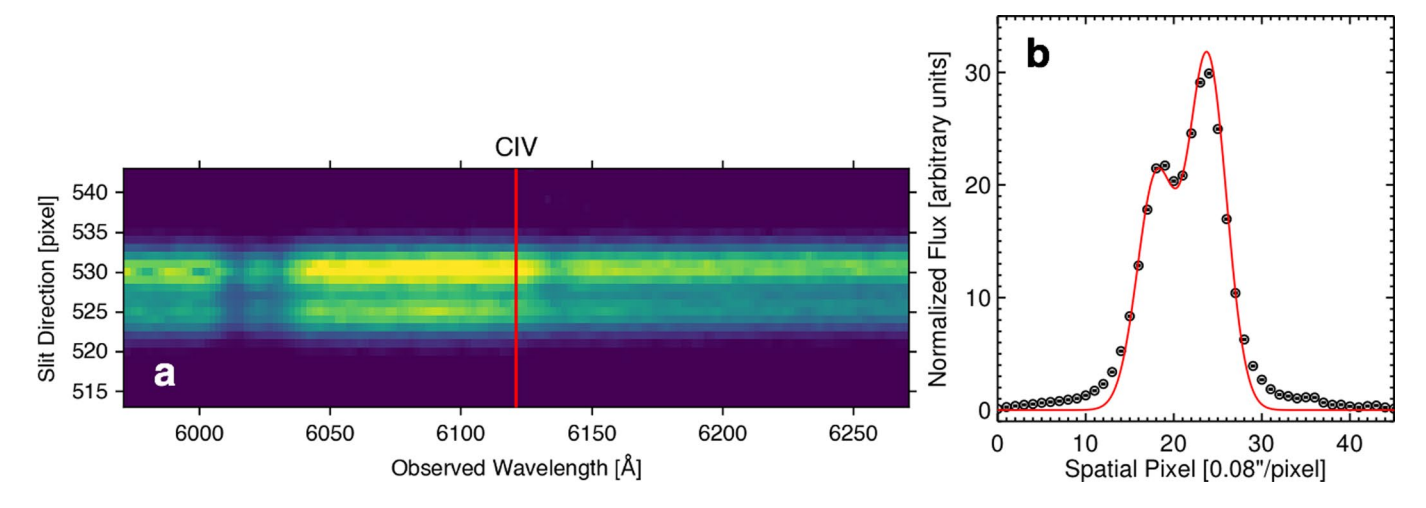




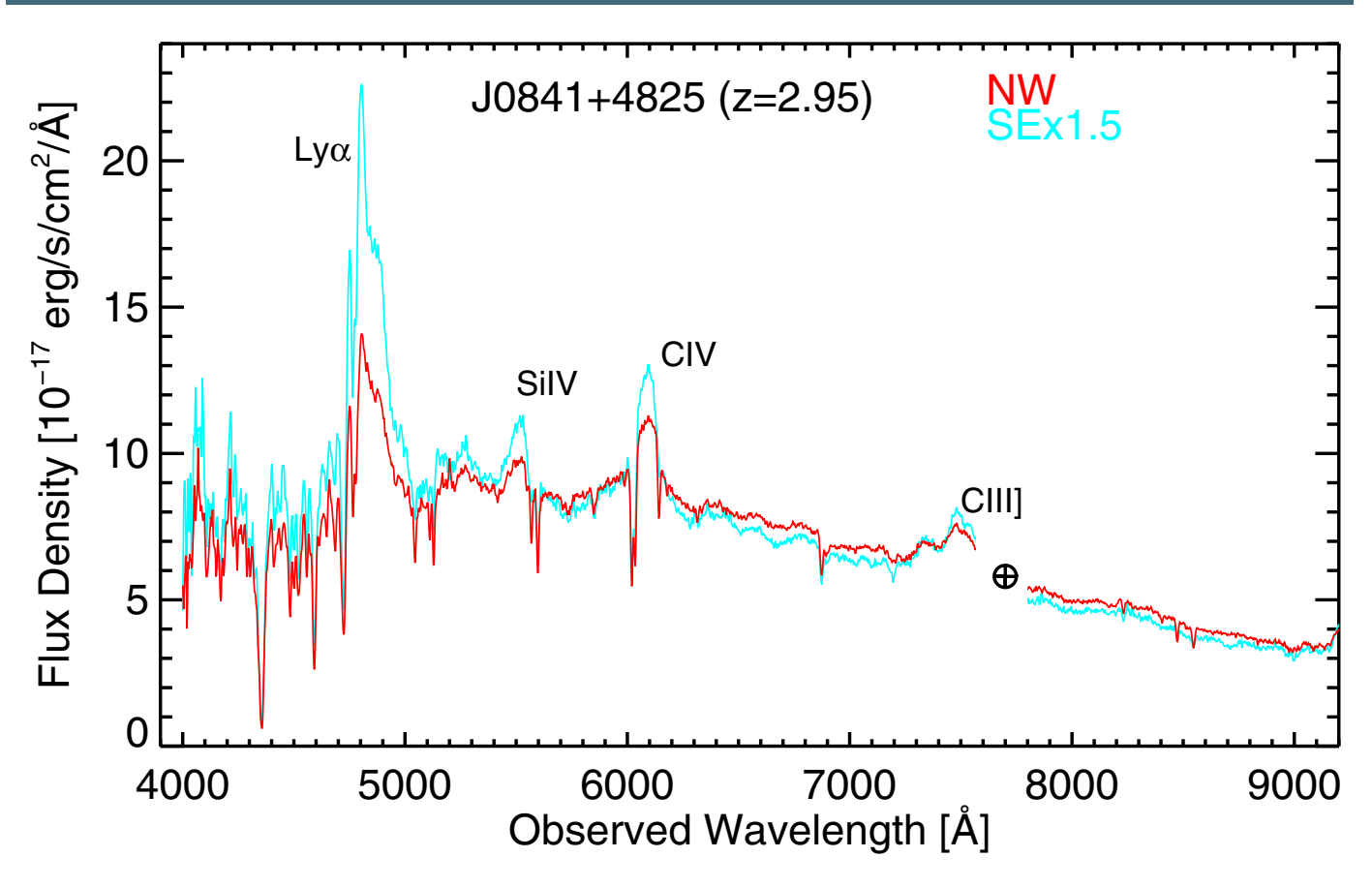
Extended Data Fig. 4 | Preliminary analysis of VLBA imaging for J0749. Panel a shows the optical HST image and panels b, c show the VLBA detection of both optical cores in Ku-band (15 GHz) with few-milliarcsec (mas) resolution, indicating both cores are quasars. There are also morphological differences in the radio images of the two cores. The VLBA beam is shown in the bottom left corner with the green ellipse.



Extended Data Fig. 5 | HST image decomposition. For each of the four systems shown in panels a-d, we show the original, model and residual (model – original) images, where the models are constructed with GALFIT. The reduced χ^2 values are provided in the lower right corner of each row.



Extended Data Fig, 6 | 2D spatial profile of J0841 in slit spectroscopy. Panel a: the two-dimensional spectrum around the CIV line, where two sources separated by $\sim 0 \cdot 46$ (-5.8 pixels) are visible. Panel b: spatial profile of the wavelength-collapsed spectrum, which we used to measure the separation between the two sources in the slit spectrum. The points are the pixel data plotted with 1σ standard deviation error bars (the errors are very small), and the red line is a double-Gaussian model.



Extended Data Fig. 7 | Spectral comparison of the two cores in J0841. The red and cyan lines are for the northwestern (NW) core and the southeastern (SE) core, respectively. The circled-cross symbol denotes the telluric absorption region masked out in the spectra. There are notable differences in the strengths of the broad emission lines after the flux of the SE core is scaled to roughly match the continuum flux of the NW core. There are also slight differences in the continuum shape and strengths in certain intervening absorption lines.